Macromolecular Rapid Communications
www.mrc-journal.de

Versatile Route for Multifunctional Aerogels Including Flaxseed Mucilage and Nanocrystals

*Abuelmagd M. Abdelmonem, Dániel Zámbó, Pascal Rusch, Anja Schlosser, Lars F. Klepzig, and Nadja C. Bigall**

Preparation of low density monolithic and free-standing organic-inorganic hybrid aerogels of various properties is demonstrated using green chemistry from a biosafe natural source (flaxseed mucilage) and freeze-casting and subsequent freeze drying. Bio-aerogels, luminescent aerogels, and magneto-responsive aerogels are obtained by combination of the flaxseed mucilage with different types of nanoparticles. Moreover, the aerogels are investigated as possible drug release systems using curcumin as a model. Various characterization techniques like thermogravimetric analysis, nitrogen physisorption, electron microscopy, UV/Vis absorption, and emission spectroscopy, bulk density, and mechanical measurements, as well as in vitro release profile measurements, are employed to investigate the obtained materials. The flaxseed-inspired organic-inorganic hybrid aerogels exhibit ultra-low densities as low as 5.6 mg cm^{-3} for 0.5% (w/v) the mucilage polymer, a specific surface area of 4 to 20 m^2 g^{-1}, high oil absorption capacity (23 g g^{-1}), and prominent compressibility. The natural biopolymer technique leads to low cost and biocompatible functional lightweight materials with tunable properties (physicochemical and mechanical) and significant potential for applications as supporting or stimuli responsive materials, carriers, reactors, microwave- and electromagnetic radiation protective (absorbing)-materials, as well as in drug delivery and oil absorption.

1. Introduction

Aerogels are a unique class of solid materials with multifold physicochemical properties, high porosity, and ultralow density derived from the sol-gel process of the molecular building blocks.[1–6] A gel is a sponge-like network structure from the corresponding nanoscopic building materials filled with a liquid. Unlike the gels, an aerogel is an effectively solid network structure with only a gas or vacuum in its pores instead of liquid.[2] Aerogels are produced by carefully extracting the pore liquid of the corresponding gel using special techniques like supercritical drying or freeze drying leaving behind a solid interconnected matrix. In this process, the liquid in the gel is replaced with a gas forming a solid material with high porosity, extremely low density, and frequently extremely low thermal conductivity, known as aerogel. Cryogelation is an aerogelation technique recently developed, widely, and successively employed in our group to prepare different types of aerogels.[7–9] In the cryogelation technique, the solution or the gel of the corresponding building blocks is first frozen followed by freeze-drying to obtain the final aerogel. The freeze drying not solely much easier to be performed compared to the supercritical CO_2 drying but it is widely available and employed in the industrial sector for diverse purposes and applications. Aerogels derived from biomaterials or natural materials are termed bio-aerogels and consist, for example, of proteins[10–14] ((e.g., gelatin, albumin, etc.) or polysaccharides

A. M. Abdelmonem, D. Zámbó, P. Rusch, A. Schlosser, L. F. Klepzig, N. C. Bigall
Institute of Physical Chemistry and Electrochemistry
Leibniz Universität Hannover
Callinstr. 3a, 30167 Hannover, Germany
E-mail: nadja.bigall@pci.uni-hannover.de

The ORCID identification number(s) for the author(s) of this article can be found under https://doi.org/10.1002/marc.202100794

DOI: 10.1002/marc.202100794

A. M. Abdelmonem, D. Zámbó, P. Rusch, A. Schlosser, L. F. Klepzig, N. C. Bigall
Laboratory of Nano and Quantum Engineering
Leibniz Universität Hannover
Schneiderberg 39, 30167 Hannover, Germany

A. M. Abdelmonem
Food Technology Research Institute
Agricultural Research Center
9 Cairo University St., Giza 12619, Egypt

D. Zámbó
Institute of Technical Physics and Materials Science
Centre for Energy Research
Konkoly-Thege M. str. 29–33, Budapest H-1121, Hungary

N. C. Bigall
Cluster of Excellence PhoenixD (Photonics, Optics, and Engineering – Innovation Across Disciplines)
Leibniz Universität Hannover
30167 Hannover, Germany

(e.g., cellulose, chitosan, alginate, starch, agar, carrageenan, etc.).[15,16] Due to their natural abundance, low cost, biodegradability, biocompatibility, eco-friendliness, and lack of (or reduced) toxicity, bio-aerogels are of exceptional importance in a wide range of applications, especially in the bio- and biomedical field.[17–20]

Flaxseed (*Linum usitatissimum L.*), also known as linseed, is one of the oldest and most widely spread crops cultivated worldwide for its different purposes like oil, fiber, and food.[21–23] Flaxseed is an excellent source of a wide range of natural compounds of special importance like oils, polysaccharides, proteins,[24–27] and antioxidants.[28–30] Due to the wide range of extractable bioactive compounds with various biological activities as antioxidant, antibacterial, antihypertensive,[31,32] and health promoting effects,[33] the flaxseeds are consumed as functional food (nutraceuticals) and for animal feeding (to promote the reproductive performance and health of the animals). Flaxseeds contain ≈28% dietary fiber of which 25–30% is soluble dietary fiber.[34] Most of the flaxseed soluble dietary fibers are located on the outside of the seed coat and known as mucilage or flaxseed gum (≈5–8% of the seed weight). The chemical composition of the flaxseed mucilage (FSM) is a mixture of polysaccharide heteropolymers composed of a mixture of acidic (rhamnogalacturonan) and neutral (arabinoxylan) polysaccharides.[35] The mucilage in general is a highly viscous, colorless liquid with good water retention gelling properties.[36] The mucilage with its unique characteristics (a good hydro-colloid with marked swelling capacity, marked water-holding capacities, and high viscosity in aqueous solution and gelling properties) as well as the natural abundance, low cost, biodegradability, biocompatibility, being eco-friendliness, and lack of (or reduced) toxicity)[36–39] have been studied for a variety of applications such as concrete additives, coacervates,[40] food industry, pharmaceutics, and drug delivery.[39–44] Comin et al. recently reported a strategy to yield FSM aerogels[45] by employing flax mucilage and barley beta-glucan. The aerogels were obtained using CO_2 supercritical dying, and their great application potential was investigated as possible delivery vehicles for nutraceuticals.

Due to the unique properties of materials in the nanoscale regime (nanoscopic features, e.g., size dependent optoelectronic properties, electronic bandgap, and the magnetic susceptibility), nanomaterials have potential applications in numerous fields such as electronics, sensing, catalysis, energy, and biomedicine.[46–52] In recent decades, the intensively growing development of synthetic methods has made it possible to produce nanoparticles (NPs) with well-controlled and precisely tailored properties. The size, shape, and surface chemistry of colloidal nanocrystals can be controlled with almost atomic precision by controlling the synthetic methods and choosing the suitable synthesis conditions (e.g., temperature, concentration of the precursors/reactants, and proper choice of ligands).[53–55]

The combination of the NPs and aerogels by grafting the NPs into the large inner surface of lightweight aerogels allows constructing macroscopic materials with nanoscopic properties. Making use of the unique properties of both NPs and aerogels promising novel functional materials can be achieved by exploiting both the large, interconnected porosity and specific surface area as well as the additional functionalities provided by the NPs.

In the present work, FSM natural polymer and freeze-drying aerogelation (as a greener alternative technique to supercritical drying) were successfully employed to prepare aerogels (bioaerogels) of different FSM concentrations. Moreover, the flax mucilage was used as a biocompatible scaffold/backbone for embedding different inorganic NPs (e.g., CdSe/CdS nanorods and magnetic IONPs) in order to prepare multifunctional hybrid (organic-inorganic hybrid) hydrogels and aerogels with distinct mechanical and physicochemical properties. This work provides a proof of concept toward a wide range of possible promising applications such as thermal insulation, catalysis, sensing, adsorbents, biomedicine (e.g., drug delivery systems, tissue engineering, and regenerative medicine, carriers, supporting or template materials, raw materials for carbon aerogels as well as organic-inorganic composite aerogels).

2. Results and Discussion

2.1. General Characterization

Physicochemical and functional properties of FSM such as high (a good hydro-colloid with marked swelling capacity, marked water-holding capacities, and high viscosity in aqueous solution and gelling properties), as well as its other features such as natural abundance, low cost, biodegradability, biocompatibility, being eco-friendliness and lack of (or reduced) toxicity are the motive power to develop advanced functional materials in field of nanotechnology and aerogels with a variety of possible applications.

As shown in **Figure 1**, monolithic, free-standing FSM bioaerogels and organic-inorganic hybrid aerogels were obtained via freeze casting (also known as ice-templating) and subsequent freeze drying). In general, the obtained aerogels had limited shrinkage and the shape of the obtained aerogels can be tuned according to the shape of templating molds (the aerogels retained their original shapes very well except for the upper or free side of the model due to the turbulences during tube during flash-freezing using the liquid nitrogen). The color appearance is white for the pure flaxseed aerogel, yellow, deep orange, and blackish for the curcumin containing aerogels, photoluminescent orange for CdSe/CdS NRs, and blackish for superparamagnetic NPs containing aerogels, respectively. While the semiconductor NR-doped aerogels show red emission under UV illumination, the superparamagnetic NP-doped ones can be attracted by a neodymium magnet against the gravity (see the results later). **Table 1** shows the bulk densities of the FSM aerogels prepared from different concentrations of the FSM polymer, curcumin loaded aerogel, and organic-inorganic hybrid aerogels (containing NPs). Obtained results shown in Table 1 indicate ultra-low density, monolithic, free-standing aerogels of densities as low as 5.6 mg cm^{-3} for 0.5% (w/v) mucilage concentration to 21.5 mg cm^{-3} corresponding to 2.0% (w/v) FSM concentration.

Monolithic free-standing aerogels were prepared also using lower FSM concentrations down to 0.1% (w/v) but data not included in the current manuscript (data were not fully characterized enough), general note for the excluded aerogels (prepared using low concentration less than 0.5% w/v) are easily compressible and easily/highly stuck (adsorbed) to other objects via electrostatic forces especially with extremely low density which makes it difficult to handle and deal. Similar phenomenon was previ-

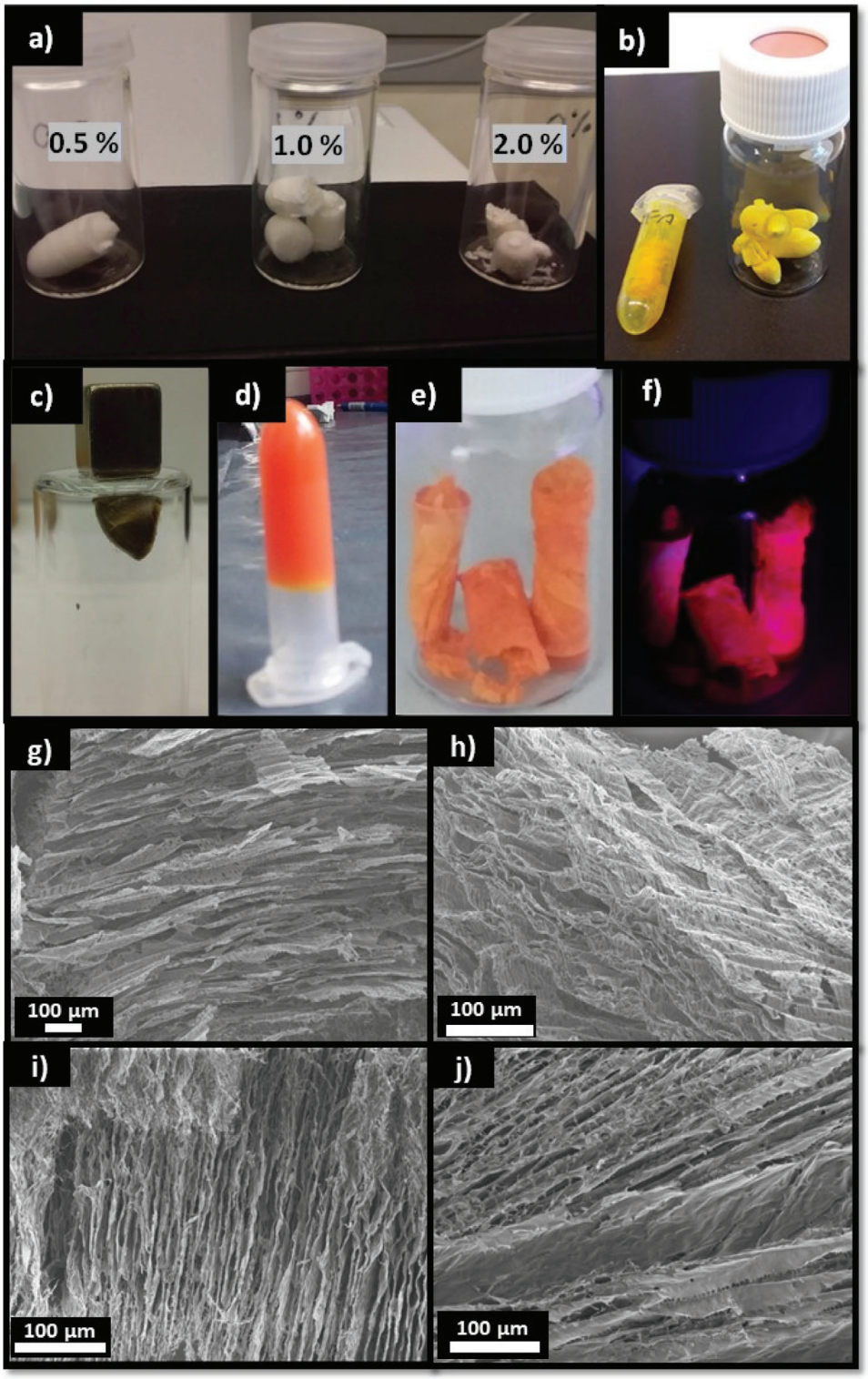

Figure 1. Photographs of a) flaxseed mucilage bio-aerogels of different concentrations, b) curcumin loaded bio-aerogel, c,d) organic inorganic (nanoparticle-loaded) hybrid aerogels. c) Magnetic or magneto responsive aerogel of flaxseed mucilage combined with iron oxide nanoparticles (IONPs, as demonstrated by interaction with a magnet), images of d) hydrogel and aerogel of fluorescent hybrid aerogels of CdSe/CdS nanorods and mucilage under e) daylight and f) UV illumination. SEM images of the morphologies of the obtained aerogels of different flaxseed mucilage concentrations: g) 0.5%, h) 1.0%, i) 1.5% and j) 2.0% (w/V). Different mechanical, morphological, and structural properties of the obtained aerogels could be further modified/controlled by controlling wide range of freezing parameters such as freezing temperature, rate, and media.[9,59–61]

Table 1. Bulk densities of the flaxseed mucilage-based aerogels.

Sample	Bulk density [mg cm^{-3}]
FAG[a] 0.5%[b]	5.6 ± 0.6
FAG 1.0%	10.6 ± 0.8
FAG 1.5%	17.3 ± 0.7
FAG 2.0%	21.5 ± 1.8
FAG-Cur[c]	19.1 ± 0.9
FAG-IONPs[d]	14.5 ± 0.5
FAG-NRs[e]	17.1 ± 1.0

[a] FAG= flaxseed mucilage aerogel; [b] (0.5, 1.0, 1.5 and 2%) indicate the mucilage concentration in the initial solution/gel; [c] Curcumin containing/loaded aerogels; [d] Magneto responsive aerogels (containing iron oxide nanoparticles); [e] Luminescent aerogels (containing CdSe/CdS nanorods).

ously reported for some aerogels of extremely low densities like cellulose nanofibers obtained aerogels.[56–58]

The morphology and structure of the FSM-based aerogels were further investigated by SEM. As displayed in Figure 1g–j and Figures S1–S4, Supporting Information, the SEM images of the obtained FSM-based aerogels show porous sheet-like laminar structures and the spacing between adjacent lamellae varies in the range of 3–25 µm. Packing density of these laminar structures increases with increasing FSM concentration from 0.5 to 2.0%.

The mechanical properties of the obtained bio-aerogels of the FSM polymer are shown in the stress–strain curves (**Figure 2**a). Similarly to the previously reported bio-inspired aerogels[62,63] the stress–strain curves consist of an elastic region at low strains followed by a stress plateau corresponding to a progressive buckling of cell walls, and the densification of the material at high strains where the stress increases abruptly. This behavior is more clearly visible for aerogels with 2.0 wt%, where the stress–strain curve exhibits small, but remarkable elastic region at lower strains followed by a stress plateau region and finally a significant densification region. Due to the less dense nature of the lamellar sheets at lower mucilage concentrations, the elastic region cannot be observed, and the structures show gradual densification upon increasing stress. Nevertheless, the FSM aerogels exhibit moderate compressibility and recovery as a function of concentration.

The thermal stability of the flaxseed-based aerogels was investigated by TGA. From the TGA measurements shown in Figure 2c,d, the first stage slight loss in mass was observed to occur up to 100 °C for all aerogels due to the loss of condensed moisture. In the second stage, the aerogels start to thermally degrade in the range of 200–433 °C due to the decomposition of the FSM. IONP-loaded aerogel shows similar thermal decomposition properties to the pristine aerogels, while the curcumin-loaded sample exhibit an additional decomposition step at 400 °C, which can be attributed to the presence of curcumin and PEG400.

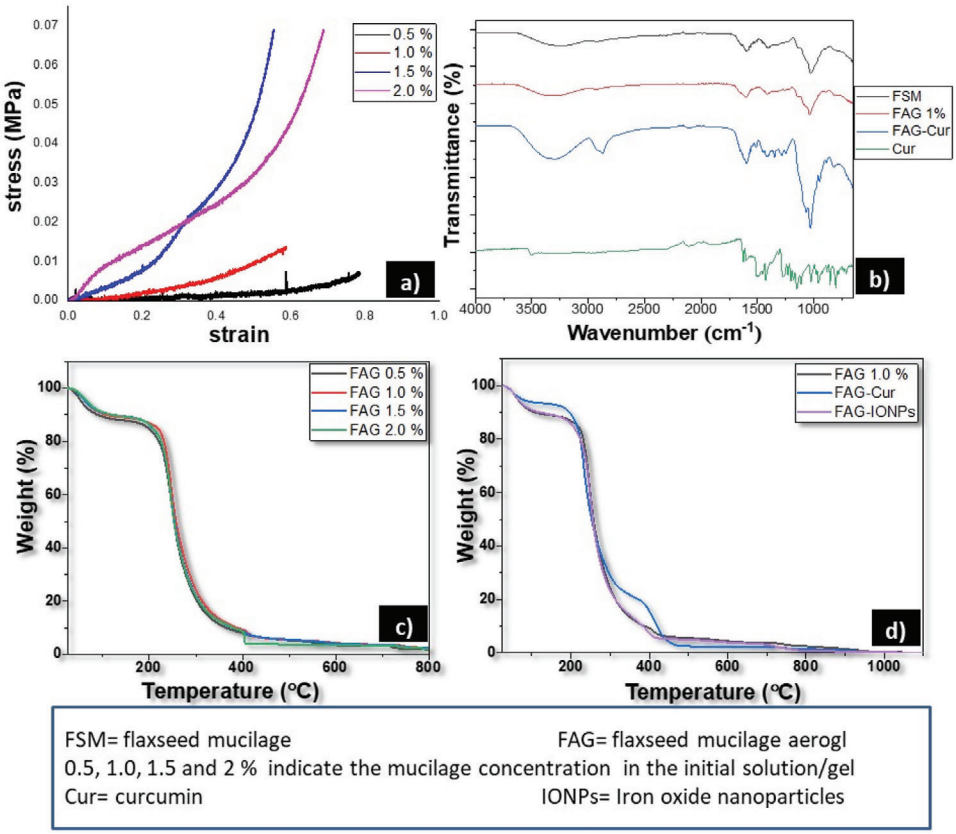

Figure 2. a) Stress–strain curves of the bio-aerogels prepared from different concentrations of the flaxseed mucilage, b) FTIR spectra of the flaxseed mucilage biopolymer, flaxseed mucilage aerogel, curcumin powder, and flaxseed aerogel containing curcumin, and c) thermogravimetric curves of the flaxseed bio-aerogels of different concentrations and d) flaxseed organic-inorganic hybrid aerogels.

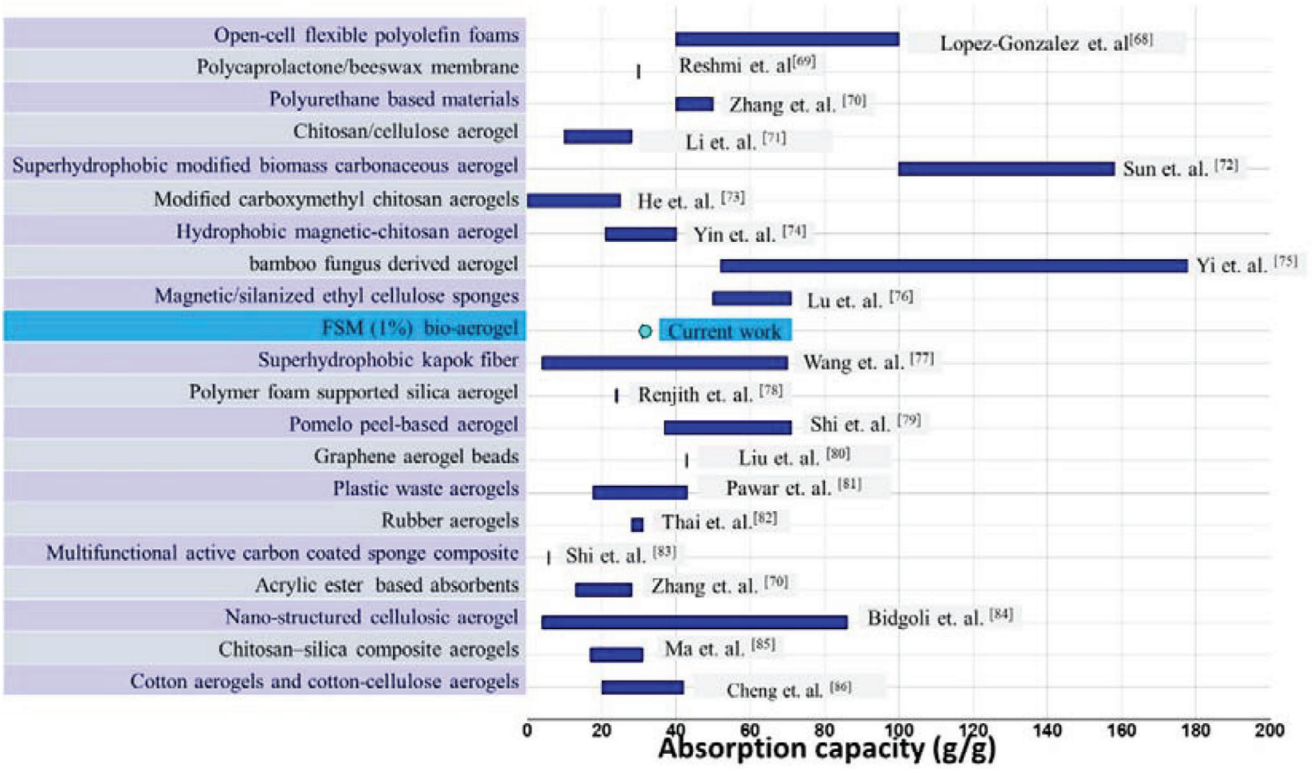

Figure 3. Chart for oil absorption capacities of some materials recently designed and investigated as highly oil-absorbents for the oil absorption applications and environmental cleaning.

Figure 2b shows the Fourier transform infrared spectroscopy (FTIR) spectra of FSM, the flaxseed-derived bio-aerogel, PEG400, the curcumin, and the curcumin-loaded flaxseed bio-aerogel in the wavenumber region of 650 to 4000 cm^{-1}. FTIR spectra of all samples containing the FSM polymer (FSM, flaxseed mucilage aerogel (FAG), and FAG-Cur) show characteristics of the FSM. The broad band observed in all sample curves at 3336 to 3500 cm^{-1} corresponds to the –OH stretching, the peak at 2937 cm^{-1} is attributed to the –C–H bonds of the CH2-CH3 groups of aliphatic chains, the peak at 1610 cm^{-1} can be attributed to the C=O stretching vibrations of galacturonic acid. The signals at 1417 and 1356 cm^{-1} could be attributed to the scissor-vibrations of the $–CH_2–$ and –OH bonds, respectively. The absorption band at 1149 cm^{-1} corresponds to the glycoside bond (C–O–C).

Additionally, a strong absorbance was observed at 1031 cm^{-1} attributed to asymmetric stretching vibrations of C–O–C bonds and two small absorption peaks at 887 and 825 cm^{-1} attributed to vibration elongation of FSM branches.[64–66] Comparing the different FTIR spectra, characteristic absorption peaks of pure curcumin at 1616, 1435, 1141 and 1025 cm^{-1} clearly contribute to the FTIR spectra of the curcumin loaded FSM aerogels.

Due to the presence of functional groups (e.g., hydroxyl and carboxylic groups), the FSM biopolymer could be of great value for the functionalization/bioconjugation and crosslinking allowing further modification and tailoring the different mechanical and physicochemical properties, functionalities, and applications in various flaxseed based materials.[64,67]

Surface area analysis via BET (Brunauer–Emmett–Teller) method and isotherm curves shown in supporting information (Figure S5 and Table S1, Supporting Information) demonstrates and, that the specific surface area of the obtained FSM bio- and hybrid aerogels is 4, 12, and 20 $m^2\ g^{-1}$ for FAG 1.5 and FAG 2.0% (bio-aerogels) and magneto responsive aerogel (organic inorganic hybrid aerogel of FSM combined with IONPs). The highest specific surface area of the FSM bio-aerogel corresponds to the highest polymer concentration (FAG 2.0%). Hybrid aerogels containing IONPs in the gel structure retain the specific surface area of the pristine backbone indicating that the incorporation of NP building blocks does not lead to a significant compression of the initial gel structure.

Oil absorption is an important area of application of the aerogels. The obtained FSM bio-aerogels showed a high oil absorption capacity of 23.5 g oil per gram bio-aerogel. This oil absorption capacity for the FAG 1% aerogel is comparable to oil absorbing capacities recently reported for some materials designed and investigated as highly oil-absorbents for the oil absorption applications and environmental cleaning (**Figure 3**). Taking into consideration that 1) not all the aerogels obtained in this work were evaluated for their oil absorption capacities but only bio-aerogel (of 1.0% FSM) and 2) this oil absorption capacity was tested using one oil (sunflower oil) as an example for the possible use of the obtained aerogels, that is, measurement of the oil absorption capacities of the obtained aerogels was not the main core of the current work. In this regard, in depth study of the different prepared

aerogels in oil absorption capacities and environmental remediation (e.g., wastewater treatment) might be of interest using different types of pollutants (e.g., heavy metals) and oils (kerosene, gasoline, motor oils, and different types of vegetable oils) and capabilities might be further enhanced by optimization different parameters.

This high oil absorption capacity of the FSM bio-aerogel might be of great value as absorbent in food applications,[87] environmental remediation[84,88] and wastewater purification as previously reported for different types of bio-aerogels such cellulose[89] and chitosan,[71] inorganic and inorganic-organic hybrid aerogels[90,91] such graphene[92,93] based aerogels.

2.2. Curcumin Loaded FSM Aerogel (FAG-Cur)

Curcumin is a yellow, low molecular weight polyphenolic natural compound obtained from rhizome of the plant Curcuma longa. Curcumin first has been extensively used as a food (turmeric and curries) for long time (centuries) in Ayurveda (traditional medicines). Recently, curcumin has gained an increased interest for applications in nutrition and medicine due to the accumulated body of evidence and recent studies reporting various health promoting and pharmacological activities of curcumin, such as anticancer[94] (for many types of cancers including colorectal, breast, lung, prostate and pancreatic carcinoma), anti-inflammatory,[95] anti-oxidant, prevention and treatment of Alzheimer's disease.[96]

Curcumin has also been investigated to develop novel materials employed in various applications in chemical sensing (colorimetric sensor for copper, hemoglobin, and pH colored sensor), drug delivery applications as carrier, radical scavengers, environmental remediation,[97] and photosensitizers in dye-sensitized solar cells (DSSC)[98–100] and photodynamic therapy.[50,101] Despite the reported broad spectrum of promising properties, the practical use of curcumin especially in bio-applications has been hampered due to its disadvantageous physicochemical properties (extremely low solubility in aqueous media, instability), poor bioavailability, and rapid metabolism. As a result of this, in order to exploit the promising properties of curcumin for the health and novel functional materials, many strategies (derivatization, conjugation, polymerization, encapsulation, and nanotechnology)[50,51,102,103] Based on the above-mentioned objectives, we employed curcumin-loaded FSM aerogel as a model system for drug delivery and controlled release with possible applications in other areas reported for the curcumin. The curcumin-loaded flaxseed polymer aerogel was successively prepared by mixing both solutions of the curcumin and the FSM. The aerogel was characterized and investigated from many aspects (optical, encapsulation efficiency (EE), loading capacity (LC), and in vitro release profile in different simulated biological fluids).

The cargo EE and LC of the developed curcumin-loaded FSM aerogel were found to be 98.65 and 5.70%, respectively. UV–vis absorption spectra (**Figure 4**) show that the specific absorption peak of curcumin becomes broader and shifts bathochromically compared to the pristine curcumin. This phenomenon can be attributed to the difference in the refractive index of the surrounding medium (water for the pristine curcumin and air and FSM for the aerogel).

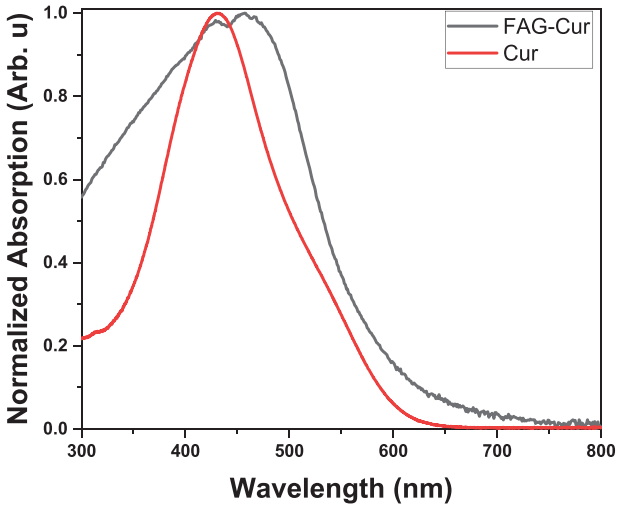

Figure 4. Normalized absorption spectra of the pristine curcumin and the curcumin-loaded flaxseed aerogel.

Due to the fast-growing interest and the need for enhanced delivery (prolonged, targeted, enhanced stability or bioavailability) of pharmaceuticals and nutraceuticals (bioactive compounds), a wide variety of novel systems have been developed and reported for the delivery through different administration routes. For the delivery purposes, the desired systems are considered to be able to precisely protect the loaded cargo (drugs or health promoting bioactive materials) during different stages and against degradation in physiological environment resulting features like enhanced stability, bioavailability, controlled drug release, minimizing adverse effects, and reducing the administered dose. Bio-based aerogels exhibit large surface to volume ratios (allowing for high drug loadings) as well as good biocompatibility, which make these architectures promising biomaterials to design drug delivery carriers.

The release profile of curcumin was investigated in vitro in two different simulated biological fluids, namely simulated gastric fluid (SGF) and simulated intestinal fluid (SIF). In order to study the release behavior of the FSM aerogel loaded with curcumin, a precisely weighted sample was immersed in SGF (pH = 1.2) or SIF (pH = 7.2) and the curcumin release was spectroscopically determined and expressed as cumulative release. As shown in **Figure 5**, the released amount changes with increasing sustained release time and for both simulated fluids (SGF and SIF), a burst release within the first 30 min for SGF and ≈2 h in the SIF can be observed. Subsequently, a sustained and slow release was observed reaching a cumulative release of 72.3% after 4 h in SGF and 54.5% after 6 h in SIF. Some biopolymers, such as mucilage have some mucoadhesive properties, which can also be used for prolonged residence/contact of drug delivery systems on the mucosal surfaces improving the prolonged drug release and delivery.[67,104]

Additionally, curcumin- FSM bio-aerogels can be of great importance as novel material for the various applications reported for curcumin in, for example, in field of DSSC,[98–100] chemical sensing, radical scavengers, environmental remediation,[97] and photodynamic therapy.[50,101]

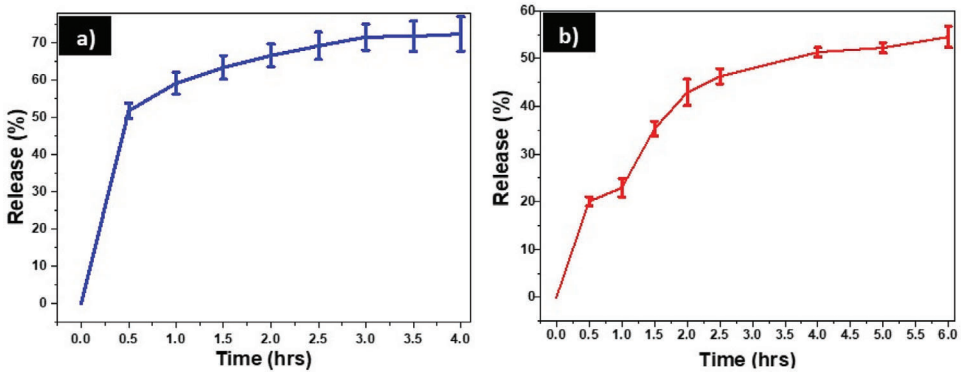

Figure 5. In vitro release profile of curcumin of the curcumin-loaded bio-aerogel in simulated biological fluids. a) Release profile in simulated gastric fluid (SGF) and b) in simulated intestinal fluid (SIF).

2.3. Organic-Inorganic Hybrid Aerogel

Immobilization of inorganic NPs like QDs in a proper matrix to develop polymer- NP hybrid composite materials is of paramount importance in a wide range of applications especially where multifunctionality is a key demand. Additionally, the grafting/immobilization of the inorganic NPs is an important means to reduce the environmental and health risk issues related to respirable particulate matter. Besides sensing, opto-electronic or photovoltaic applications, QD containing aerogels have been successfully employed in 3D displays.[105] Applications, mechanical and physicochemical properties of such polymer-NP hybrid materials have been extensively explored.[105,106]

Being monolithic, free-standing, and prepared from low concentration as well as the ease of preparation, FSM bio-aerogels could be of great importance to be combined with inorganic NPs enhancing and tailoring the mechanical and voluminous properties nanoscopic features of the NPs into macroscopic world. Here, organic-inorganic hybrid aerogel materials were developed from FSM polymer and different types of inorganic NPs to demonstrate the versatility of the bio-aerogel backbone toward multifunctional aerogel structures.

2.3.1. Luminescent Aerogels

Luminescent organic-inorganic hybrid aerogels were prepared via embedding the luminescent CdSe/CdS nanorods in the flaxseed derived biopolymer (mucilage). **Figure 6** shows the morphology of the as-synthesized NRs as well as the hybrid aerogels. CdSe/CdS nanorods (Figure 6a) prepared by seeded growth in organic solvent were transferred into aqueous phase by ligand exchange phase transfer using mercaptopropionic acid then mixed with the flaxseed polymer solution to prepare the luminescent organic-inorganic hybrid aerogel. TEM images of the luminescent organic-inorganic hybrid aerogel containing the CdSe/CdS nanorods (Figure 6b–f) show that the nanorods retain their morphology and are spatially distributed upon embedding in the biopolymer matrix, which is a key requirement to preserve their nanoscopic optical properties. During the formation of the sheet-like structures upon flash-freezing, the nanorods become confined in the laminar structures. Agglomeration or structural destruction was not observed in the hybrid aerogels.

Optical properties (absorption and photoluminescence spectra, fluorescence decay, and PL quantum yields) of the CdSe/CdS nanorods and the obtained luminescent organic-inorganic hybrid aerogel are shown in **Figure 7**. Photoluminescence measurements (PL spectra in Figure 7b) indicate, that the peak positions (λ_{max}) of the hydrophobically capped CdSe/CdS nanorods in toluene, water soluble mercaptopropionic acid capped CdSe/CdS nanorods and the organic-inorganic hybrid aerogels containing the CdSe/CdS nanorods are located at 606, 601 and 628 nm, respectively. This implies, that the aerogelation causes a prominent bathochromic shift (≈27 and 22 nm) compared to the peak positions of the NP solutions for the CdSe/CdS nanorods in toluene, and in water, respectively. Similarly as discussed above for curcumin-loaded aerogels, these spectral changes, can be attributed to the refractive index change of the surrounding medium (toluene, water, and air).[107] Additionally, regarding the photoluminescence spectra, self-absorption in these hybrid aerogel samples (due to the high NR concentration in a certain volume) has to be taken into account, which may contribute to the bathochomic shift.

In order to get a clearer picture of the radiative recombination of the charge carriers, the fluorescence lifetime was recorded for NRs in solutions (in toluene and in water) as well as in the organic-inorganic hybrid aerogel. Lifetime decay curves and the corresponding average lifetimes of CdSe/CdS NRs in the three different matrices are shown in Figure 7c,d and in Table S2, Supporting Information. The average exciton lifetimes were found to be 15.4 ns for the pristine hydrophobically capped CdSe/CdSe NRs in the organic solvent (toluene), 8.7 ns for the water transferred CdSe/CdS NRs (MPA capped), and 14.0 ns for the FSM -CdSe/CdS hybrid aerogels. Replacing the original TOP/TOPO ligands of the NRs by surface grafted thiolated molecules (MPA) causes shortening in exciton lifetimes, which can be attributed to the generated hole traps or less-covered surface defects upon grafting by thiols via opening new, non-radiative channels. However, embedding the NRs in the biopolymer gel leads to the elongation of the exciton lifetimes closer to the value in toluene, meaning that the particles might regain the majority of the originally existed radiative channels which can be explained by the reducing the non-radiative recombination pathways in aero-

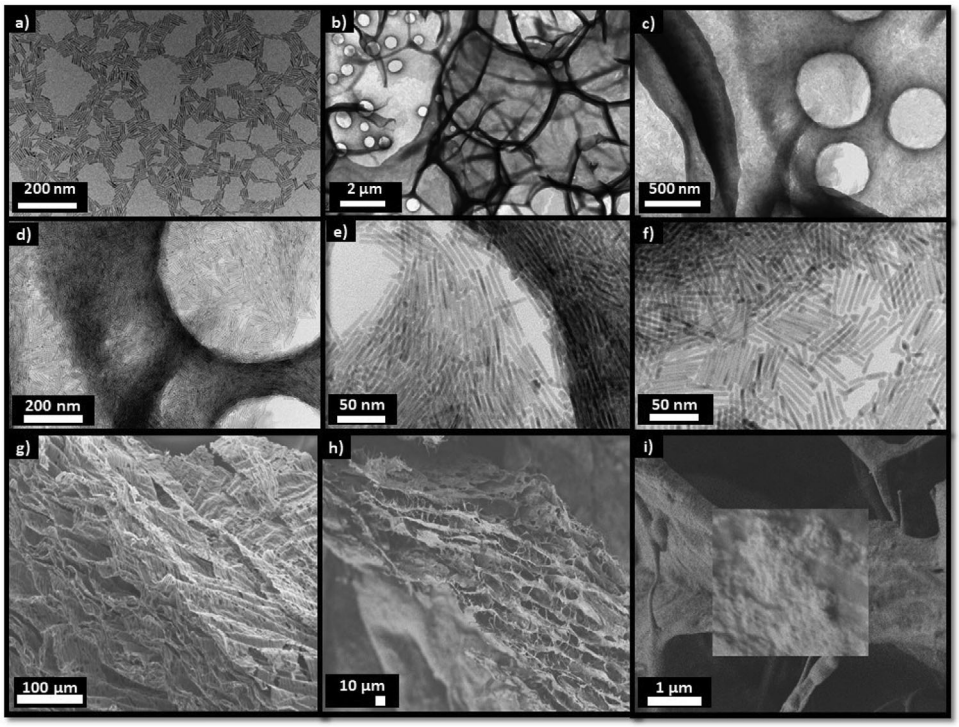

Figure 6. TEM images of a) the CdSe/CdS NRs in toluene and b–f) CdSe/CdS mucilage hybrid aerogels at different magnifications and SEM images of g) the pure mucilage bio-aerogel and h,i) CdSe/CdS mucilage hybrid aerogels.

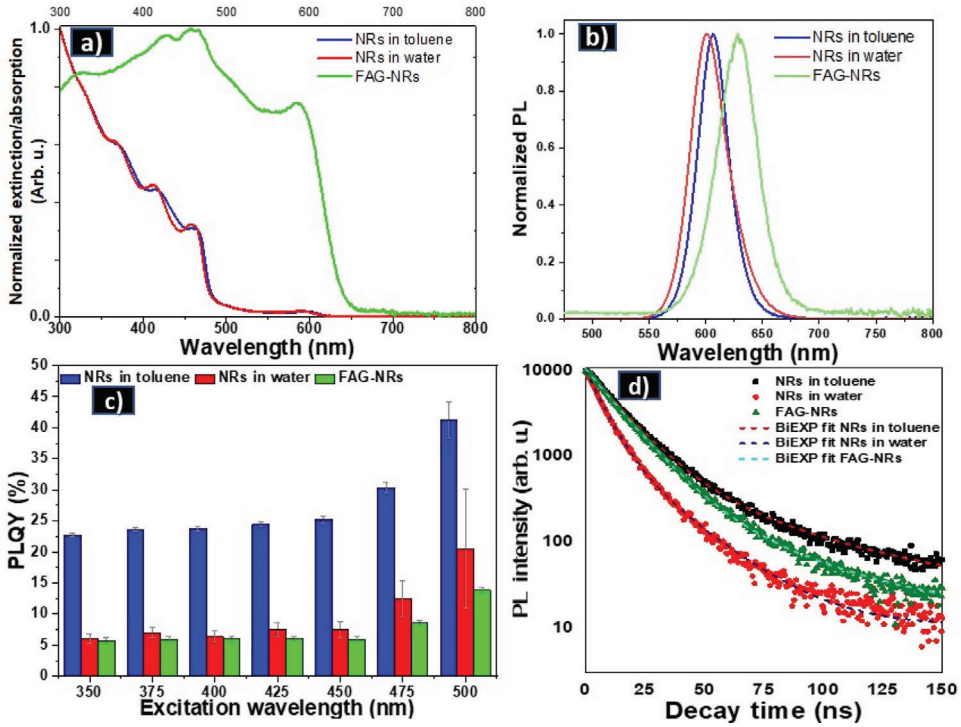

Figure 7. a) Normalized extinction for solutions (NRs in toluene and MPA capped NRs in water), absorption for solid sample (FAG-NRs aerogel), b) photoluminescence spectra of the hydrophobically capped (blue lines) CdSe/CdS nanorods in toluene, water soluble (red lines) mercaptopropionic acid capped CdSe/CdS nanorods and the organic-inorganic hybrid aerogels (green lines) containing the CdSe/CdS nanorods, c) photoluminescence quantum yields and d) lifetime decay curves of the CdSe/CdS NRs in toluene, water soluble (MPA capped) and CdSe/CdS NRs-organic hybrid flaxseed aerogel.

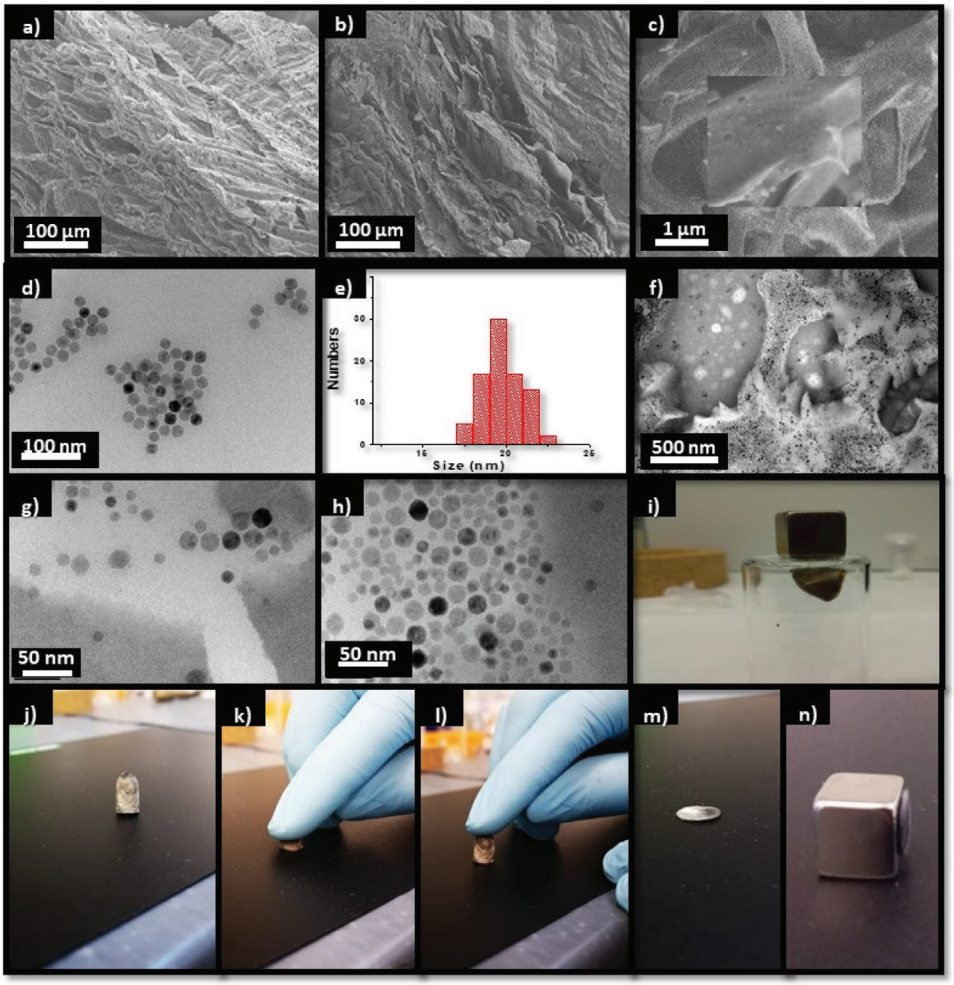

Figure 8. SEM images of a) the pure mucilage aerogel and b,c) the magnetic organic-inorganic hybrid aerogel combined of the flaxseed mucilage aerogel and the iron oxide nanoparticles. d) TEM image and e) size distribution of the iron oxide nanoparticles. f–h) TEM images of the magnetic organic-inorganic hybrid aerogel combined of the flaxseed mucilage aerogel and the iron oxide nanoparticles. i) Response of the hybrid aerogel to an external magnetic field. j–n) Compressibility and deformability of the hybrid bio-based aerogel.

gels compared to the liquid environment as has been previously seen.[108] In addition, this phenomenon might be explained by a better passivation of the particles in the biopolymer matrix in air environment compared to the aqueous environment of the water-transferred solution. TEM images (Figure 6e,f) show separately present NRs in the biopolymer matrix, demonstrating the preservation of original NP morphology upon embedding the nanorods in the biopolymer. Consequently, NRs can retain their fluorescent properties in the FSM matrix as the PLQY values also clearly demonstrate (Figure 7c): QY values of the hybrid aerogels are similar to the values of MPA-grafted NRs in water. Thus, photophysical measurements prove, that the obtained luminescent organic-NR aerogel provides retained photophysical properties which makes these macroscopic aerogel structures a promising platform for novel multifunctional materials especially for 3D networks, sensing, and catalysis.

The developed luminescent hybrid (organic-QRs) aerogels are ultralight monolithic materials that could overcome drawbacks such as poor mechanical stability, handling issues, health- and environmental-related risks of conventional, inorganic QRs macroassemblies.[107]

2.3.2. Ultralight Magnetic Organic-Inorganic Hybrid Aerogel

As magnetic nanomaterials and their composites have been investigated for biomedical, data storage, and device applications, magnetic aerogels are of great importance in various aspects of applications from microfluidic devices to electronic actuators.[109,110]

Caffeic acid capped magnetic IONPs embedded in FSM matrix were employed to obtain ultralight magnetic porous aerogels. **Figure 8** shows the TEM images of the caffeic acid capped IONPs and their size distribution (Figure 8d,e) as well as the FSM aerogel containing the magnetic NPs (Figure 8f–h). The prepared hybrid aerogel possesses numerous advantageous properties such as magneto responsivity, deformability/recoverability as shown in the bottom panel of Figure 8.

The applied straightforward and green strategy opens routes toward novel biocompatible ultralight multifunctional magnetic NP-based aerogel materials merging the properties of the magnetic building blocks as well as the bio-derived matrix. The obtained magnetic aerogel exhibits the advantages of the lightweight aerogel backbone and the sensitivity of the NPs to magnetic stimulus that make these materials a promising candidate for many potential applications reported of magnetic aerogels in the fields of monolithic magnetic actuators, microwave and electromagnetic radiation protective (absorbing) materials,[111] environmental remediation like oil absorption,[112–114] heavy metals and pollutants removal,[115,116] microswitches, smart and lightweight applications.

3. Conclusion

This work provides a general strategy for fabricating ultralow-density functional materials with tailorable properties and functionalities based on the combination of a widespread, biocompatible, food grade natural biopolymer and a low cost and CO_2-reduced preparation technique toward a wide range of possible applications. FSM, a natural biopolymer was employed to prepare ultra-lightweight monolithic free-standing bio-aerogels and organic-inorganic hybrid bio-based aerogels using a simple technique widely employed in food and pharmaceutical applications (flash freezing and subsequent freeze drying) and recently also as cryogelation for NP aerogelation. The structure and properties of the bio-based aerogel matrix were optimized as a function of the biopolymer concentration. Loading and release of the FSM bio-based aerogel were carried out with curcumin as a proof of concept for the potential application in drug release. Furthermore, the bio-aerogel was found to be an efficient oil absorber.

Additionally, FSM and different types of NPs (magnetic IONPs and luminescent CdSe/CdS NRs) were combined to fabricate novel multifunctional organic-inorganic hybrid materials merging the advantageous properties of nanomaterials (superparamagnetism and fluorescence) with those of the aerogel matrix. These novel, ultralight, organic-inorganic bio-based materials with their enhanced/controlled physicochemical and mechanical properties provide a platform to overcome the longstanding obstacles of the inorganic NPs such as poor handling properties, health, and environment related issues.

Concluding, combining the FSM biopolymer with a green aerogelation technique (freeze-casting and freeze drying) allows to prepare low cost and biocompatible functional lightweight materials of tunable properties (physicochemical, mechanical, and biological) with a wide range of possible applications as supporting materials, carrier, drug delivery, stimuli-responsive materials, reactor, and oil absorption.

4. Experimental Section

Reagents and Materials: Iron (III) chloride hexahydrate ($FeCl_3 \cdot 6H_2O$, ≥99%), caffeic acid (≥98.0), polyethylene glycol 400 (PEG 400, ≥99%), tri-*n*-octylphosphine oxide (TOPO, 99%), elemental sulfur (99.98%), 1-octadecene (ODE, 90%), 3-mercaptopropionic acid (MPA, ≥99%), and chloroform (≥99.5%) were purchased from Sigma Aldrich. Potassium hydroxide (KOH, >85%), toluene (≥99.7%), acetone (99.5%), *n*-hexane (≥99%) and methanol (MeOH, ≥99.8%) were purchased from Honeywell. Ethanol (EtOH, ≥99.8%) and curcumin (≥90%) were obtained from Carl-Roth. Hexylphosphonic acid (HPA, 99%) and octadecylphosphonic acid (ODPA, 99.0%) were obtained from PCI. Tri-*n*-octylphosphine (TOP, 97%) was purchased from ABCR. Cadmium oxide (CdO, 99.998%), elemental selenium (powder 200 mesh, 99.999%), and oleic acid (OLA, > 90%) were supplied by Alfa Aesar. Flaxseeds were obtained from the local market (Rossmann GmbH, Germany).

All chemicals were used as received without any further purification. Ultrapure water (resistivity of 18.2 MΩ·cm) was used for all the aqueous solutions.

FSM Biopolymer Extraction: The FSM was extracted by the hot water extraction followed by the centrifugation and drying as previously described with little modifications as follows. The whole flaxseeds (100 g in 900 mL Millipore water, 1:9 ratio) were heated to 65 °C and extracted at this temperature for 4 h under magnetic stirring (800 rpm). Subsequently, the flaxseed solution was separated from the seed by filtering through cotton cheesecloth. Later, the FSM was precipitated by addition of ethanol (1:1 to the solution) and centrifuged at 38 600 rcf and 4 °C. The collected FSM was dried in an oven at 80 °C, ground, and kept in small vials until further use.

Synthesis of IONPs and Water Transfer via Ligand Exchange: The oleic acid capped magnetic IONPs were prepared by thermal decomposition of iron (III) oleate based on a previously reported procedure[117] with some modifications. For the preparation of the iron oleate, iron (III) chloride hexahydrate (12 mmol, 3.24 g) and sodium oleate (36 mmol) were dissolved in a mixture of solvents consisting of ethanol (24 mL), water (18 mL), and hexane (42 mL). The mixture was heated to 70 °C and magnetically stirred for 4 h in a round bottom flask equipped with a condenser. The mixture was cooled to room temperature, transferred to a separatory funnel where the aqueous layer was discarded, and the product was washed three times with water. The organic layer containing the iron oleate complex was transferred to a rotary evaporator and the organic solvents were removed by evaporation under reduced pressure leaving the iron oleate complex as a viscous product.

For the oleic acid capped IONPs, the previously prepared iron oleate complex (8 mmol, 7.202 g) and oleic acid (4 mmol, 1.13 g) were dissolved in octadecene (40 g) in a 3-neck round bottom flask. The mixture was degassed for 30 min at 100 °C then heated to 320 °C for 1 h under argon and finally the heating mantle was removed so that the NP solution was cooled to room temperature. Toluene (20 mL) was added and the IONPs were precipitated by adding an equal volume of ethanol and collected by centrifugation at 3900 rcf for 10 min. The NPs were dispersed in toluene and cleaned again by ethanol and centrifuging. The final oleic acid capped magnetic IONPs were dispersed in 16 mL anhydrous chloroform.

Water Transfer of the Magnetic Iron Oxide: The oleic acid capped magnetic IONPs were transferred to aqueous solution via ligand exchange with caffeic acid as reported before[118] with minor modifications. First, 5 mL of the IONPs were precipitated by addition of methanol (2 mL) and centrifugation at 3900 rcf for 10 min and the obtained NPs were dispersed in toluene. Caffeic acid (80 mg in 3.2 mL water and 800 µL NaOH, 1 M) was added to 4 mL of IONPs (20 mg in toluene). The mixture was vortexed, sonicated for 10 min, and then agitated by orbital shaker for 3 days. Subsequently the NPs were extracted by centrifugation for 10 min at 5000 rpm and dispersed in 10 mL Millipore water.

Synthesis of CdSe/CdS Nanorods and Ligand Exchange: The CdSe/CdS nanorods (NRs) were prepared by the seeded-growth hot injection method (CdSe seed synthesis and subsequent growth of the rods).[119] The synthesis was based on the anisotropic growth of CdS over the previously prepared spherical, hexagonal CdSe quantum dots.

CdSe Seeds: In the first stage CdSe seeds were prepared following the procedure of Carbone et al. with minor modifications.[119] Typically, a mixture of trioctylphosphine oxide (TOPO, 6.0 g), octadecyl phosphonic acid (ODPA, 0.560 g), and CdO (0.120 g) in a 50 mL 3-neck round bottom flask was degassed under vacuum at 150 °C for 1 h. Then, under argon, the mixture was heated to 300 °C until the complete dissolution of CdO (a clear and colorless solution was obtained). Trioctylphosphine (TOP, 1.8 mL) was injected into the flask, and the temperature was increased

to 380 °C. At this temperature, Se:TOP solution (0.116 g Se dissolved in 3.8 mL TOP) was quickly injected. After 4 min, the heating mantle was removed and ODE (10 mL) was immediately injected. At 80 °C, toluene (10 mL) was added and the NPs were precipitated with methanol and centrifuged at 3800 rcf. The NPs were redispersed in toluene followed by addition of methanol and centrifugation at 3800 rcf. The washing step (redissolution in toluene and precipitation by the addition of methanol) was repeated twice and the obtained CdSe NPs were finally dissolved in toluene (1.5 mL).

CdSe/CdS Rod Growth: In a second step, the anisotropic growth of CdS onto the CdSe seeds was performed according to the above-mentioned work. Typically, in 3-neck round bottom flask, CdO (0.060 g), TOPO (3.0 g), ODPA (0.280 g), and hexylphosponic acid (HPA, 0.080 g) were melted and degassed under vacuum for ≈1 h at 150 °C. Then the mixture was heated up to 300 °C under argon and 1.8 mL of TOP was injected and the resulting solution was further heated to 380 °C under argon. At this point, the TOP:S precursor solution (0.130 g S dissolved in 1.8 mL TOP), in which the required amount CdSe seeds (to reach 400 µM of CdSe QDs in the total growth solution) in minimum amount of toluene was dissolved, was quickly injected. After injection, the temperature dropped to ≈270–300 °C and the solution was left to recover the temperature for 8 min. After 8 min, the heating mantle was removed and the solution cooled down to the room temperature. In the meantime, toluene (10 mL) was injected at 80 °C. The CdSe/CdS nanorods were purified three times via centrifugation-redispersion cycles (precipitation by methanol, redispersion in toluene) and the purified nanorods were finally stored in toluene (4.5 mL).

Water Transfer of Semiconductor NPs (Ligand Exchange): To transfer the CdSe/CdS semiconductor NPs from organic solution to aqueous media, ligand exchange was carried out following the procedure published by Kodanek et al.[120] CdSe/CdS rods (4.5 mL in toluene) were precipitated by adding MeOH, centrifuged at 3800 rcf and the collected particles were redispersed in hexane (6 mL). The transfer solution of mercaptopropionic acid (consisting of 15 mL MeOH, 0.32 g KOH, and 0.388 mL 3-MPA) was added to the CdSe/CdS solution followed by shaking on an orbital shaker overnight. The two phases were allowed to be separated and the aqueous layer containing the transferred NPs was collected and centrifuged (3600 rcf, 3 min). The particles were redispersed in KOH solution (0.1 M, 6 mL). Organic residue was removed by adding chloroform (1.5 mL) to the nanorods solution followed by vortexing and centrifugation (at 3600 rcf for 5 min repeated twice). Finally, the CdSe/CdS particles were redispersed in aqueous KOH solution (0.1 M, 6 mL).

Hydrogel and Aerogel Preparation: For the preparation of the FSM gel of different concentrations (wt%), the FSM powder was added and hydrated in water (in different concentrations, wt%) forming aggregated inhomogeneous gels due to the high viscosity of the FSM. Heating and water bath sonication were employed for the dissolution and homogenization of the hydrated FSM. The mucilage solution mixture was heated for 3 h at 65 °C in a water sonication bath. Due to the high viscosity, the dissolution (or more accurately the homogeneous hydration) of the flax seed mucilage was very problematic especially at higher concentrations despite applying heating at 80 °C and sonication for 4 h. Due to its high viscosity and inhomogeneous hydration, the highest concentration used here was 2.0%. The obtained hot (60 °C) gels of different concentrations (0.5, 1.0, 1.5 and 2.0%) were transferred to the mold (Eppendorf tube or 3 mL plastic syringe) and covered with a lid (or Parafilm in case of the plastic syringe) to avoid any moisture loss.

For the aerogelation, the molds containing the FSM gels were immersed in liquid nitrogen then freeze-dried (Christ Freeze Dryer LD 1-2 plus) for 24 h with a pressure of 0.011 mbar. The obtained FSM aerogels were termed FAG 0.5%, FAG 1.0%, FAG 1.5% and FAG 2.0% corresponding to 0.5, 1.0, 1.5 and 2.0% mucilage concentrations.

Organic-Inorganic Hybrid Aerogels Preparation: For the organic-inorganic hybrid aerogels, 500 µL of the aqueous inorganic NPs solutions (6.5 mg mL^{-1} for CdSe/CdS nanorods and 4.0 mg mL^{-1} for IONPs) were added to hot (60 °C) FSM solution (500 µL, 2.0 wt%). The mixture was vortexed to obtain a homogeneous solution (gel) and the organic-inorganic aerogels were prepared via freeze-drying as described above for the FSM bio-aerogels to obtain luminescent CdSe/CdS bio-hybrid aerogel (FAG-NRs) and magnetic IONPs FSM bio-hybrid aerogel (FAG-IONPs).

Curcumin Loaded Aerogel and Drug Release: Curcumin loaded aerogel was prepared with 1.0% FSM as follows, a solution of FSM was prepared as mentioned above. Curcumin has very low water solubility, therefore polyethylene glycol 400 (PEG 400) was used as solvent for the curcumin due to the high solubility of the curcumin in PEG 400 (100 mg mL^{-1}) as reported previously.[121] For the hydrogel preparation, solution of 5 µL of curcumin solution (200 mg mL^{-1} in PEG 400) was mixed to 995 µL FSM solution (500 µL mucilage solution 2.0 wt% and 495 µL Millipore water). The curcumin loaded FSM bio-aerogels were prepared as previously described by freeze drying.

Bulk Density Measurements: For the bulk density measurements of the obtained aerogels, mass and volume of the aerogels were measured, thus bulk densities of the aerogels can be calculated by the following equation:

$$\rho = \frac{m}{V} \tag{1}$$

where m is the mass (mg) of the sample and V is the volume.

Materials Optical Characterization: NP solutions (in organic solvent or water) as well as hydrogels were spectroscopically characterized in 4 mm path length (semi-micro) or 2 mm path length (micro) quartz cuvettes. Absorption spectra were measured using a Jasco V750 UV/Vis spectrometer, the photoluminescence (PL) spectra, and the lifetime measurements (time-correlated single photon counting, TCSPC) were carried out using a Horiba Fluoromax-4 spectrofluorometer. Photoluminescence quantum yields (PLQYs) were determined using a Horiba Dual-FL spectrofluorometer equipped with a Quanta-ϕ integrating sphere.

For the solid materials (aerogels), the absorbance spectra and PL quantum yield measurements were obtained by a Quanta-ϕ integrating sphere coupled to a Horiba Dual-FL spectrofluorometer and the PL spectra and the lifetime measurements (time-correlated single photon counting, TCSPC) were carried out using a Horiba Fluoromax-4 spectrofluorometer equipped with a Horiba Nano LED light source and Fluorohub controlling system (λ_{exc} = 454 nm). The optical measurements were performed in a Teflon sample holder (1 cm in diameter and 3 mm in depth) equipped with a quartz coverslip.

Structural Characterization: Scanning electron microscopy: samples were prepared by immobilizing pieces of aerogels on conductive carbon tapes, and the SEM images were taken by a JEOL JSM-6700F (operated at 2 kV) scanning electron microscope.

Transmission electron microscopy: for the TEM image, copper grids covered with a carbon layer (Quantifoil) were used, and the samples were prepared by drop-casting (in case of NP solutions or hydrogels) or by pulling the grids on the surface of the aerogels gently. The TEM images were recorded by a FEI Tecnai G2 F20 TMP (operated at 200 kV) transmission electron microscope.

Mechanical Measurements: Compression tests on the aerogels were performed using an Instron 5565A. Cylindrical test samples with 9.6 mm diameter and 11 to 15 mm height were produced by gelation in cylindrical glass molds. These samples were compressed at a steady rate of 0.2 mm s^{-1} while measuring the resulting force and the experiment was stopped once a force of 5 N was reached. The stress and strain were calculated using the initial contact area of monolith and plate and the initial height of the monolith, respectively.

Thermogravimetric Analysis (TGA): Thermogravimetric analysis of the aerogels was carried out using a Mettler–Toledo TGA/DSC 3+ with the aerogel samples loaded into 300 µL alumina crucibles. The samples were heated from room temperature at 2 K min^{-1} rate under a flow of air (50 mL min^{-1}).

FTIR: FTIR was used for chemical characterization and detection of the possible interactions. FTIR spectral analysis of flaxseed-based materials was carried out by an FTIR Spectrophotometer (Agilent Technologies Cary 630 FTIR) in the range of 4000–650 cm^{-1}.

Nitrogen Physisorption Measurements: Specific surface area and porosity analysis were carried out with the N2 physisorption method. For the measurements, glass measurement cells were well cleaned, dried, and

weighted. A proper amount of the sample (aerogel) was placed in the glass cells (of a known weight) and degassed at 100 mbar at room temperature for 24 h. On the next day, the glass cells containing the dry (degassed) aerogel samples were weighed again, and the mass of the aerogel sample was calculated and noted as the difference between the weight of the empty glass cell and the weight of the cell and the degassed samples. The N2 physisorption measurements of the degassed aerogel samples were performed on a Quantachrome Nova 3200e series instrument using nitrogen as gaseous adsorbate.

Oil Absorption: FSM aerogel (FAG 1.5%) was used to study the oil absorption capacity of the obtained aerogel. For this purpose, a precisely weighted amount of the flaxseed aerogel was immersed in sunflower oil for 20 min then removed and put on a filter paper to remove the extra oil. Finally, the sample was weighed and the oil absorption capacity was calculated as follows:

$$Q = \frac{m_s - m_0}{m_0} \tag{2}$$

where, Q is the oil absorption capacity in g g^{-1}, m_0, m_s are the weight of the FSM aerogel before and after the oil absorption, respectively.

EE and LC: The EE and LC of the curcumin were spectrophotometrically determined using standard curve according to the following equations:

$$EE = \frac{\text{Amount of the drug in aerogel}}{\text{Initial amount of the drug used}} \times 100 \tag{3}$$

$$LC = \frac{\text{Amount (weight) of the drug in aerogel}}{\text{Total weight of the drug used}} \times 100 \tag{4}$$

In Vitro Release Profile (Drug Delivery and Stimulated Release): The release profile of the curcumin loaded FSM aerogel was investigated in two different biologically simulated fluids (SGF and SIF) prepared as previously reported.[122]

The SGF was prepared as follows, for 1 L volume of the SGF, 3.2 g pepsin was added to a solution of hydrochloric acid solution (7 mL, 0.2 M) and sodium chloride (2.0 g) in 950 mL water. The pH was adjusted to 1.2 and then the final volume was topped to 1000 mL with Millipore water.

For the SIF, and for 1 L volume, 10 g pancreatin, monobasic potassium phosphate (50 mmol, 6.8 g), and sodium hydroxide (0.6 g) solution was dissolved in 950 mL water. The final pH of SIF was adjusted to 6.8 and the total volume to 1 liter with Millipore water.

For the release profile measurement, certain amount of the curcumin loaded bio-aerogel was mixed with 40 mL of SGF or SIF and incubated at 37 °C. At the preset time points (0.5, 1, 2, 4, and 8 h), 2 mL aliquots were withdrawn, centrifuged at 3600 rcf for 5 min, and extracted in acetone. The absorption at 424 nm was recorded. The concentration of the curcumin was determined from calibration standard curve of serial dilutions of standard curcumin used in calculations, and data were expressed as cumulative drug release at different time points.

Supporting Information

Supporting Information is available from the Wiley Online Library or from the author.

Acknowledgements

The authors would like to acknowledge the European Research Council (ERC) under the European Union's Horizon 2020 research and innovation program (Grant agreement 714429). The project leading to these results has in part by the German Research Foundation (Deutsche Forschungsgemeinschaft, DFG) under Germany's excellence strategy within the cluster of excellence PhoenixD (EXC 2122, project ID 390833453) and the grant BI 1708/4-1. In addition, this work was funded by the Hannover School for Nanotechnology (hsn). The authors would like to thank the Laboratory of Nano and Quantum Engineering for the use of the TEM and Prof. Armin Feldhoff for providing the SEM facilities. The authors would to express special thanks to the grant financed by the Science, Technology & Innovation Funding Authority, (Grant no. 37041, STDF, Egypt) and GERSS program (joint scholarship program between the Ministry of Higher Education Egypt, MHESR and the German Academic Exchange Service, DAAD, Germany). D.Z. acknowledges the program financed by the National Research, Development and Innovation Office of the Ministry for Innovation and Technology, Hungary (TKP2021-NKTA-05)

Open access funding enabled and organized by Projekt DEAL.

Conflict of Interest

The authors declare no conflict of interest.

Data Availability Statement

The data that support the findings of this study are available from the corresponding author upon reasonable request.

Keywords

aerogels, biopolymers, cryogels, flaxseed mucilage, hybrid nanostructures, nanoparticles

Received: December 13, 2021
Revised: January 14, 2022
Published online:

[1] S. S. Kistler, *Nature* **1931**, *127*, 741.
[2] N. Hüsing, U. Schubert, *Angew. Chem., Int. Ed.* **1998**, *37*, 22.
[3] J. L. Mohanan, I. U. Arachchige, S. L. Brock, *Science* **2005**, *307*, 397.
[4] C. Ziegler, A. Wolf, W. Liu, A.-K. Herrmann, N. Gaponik, A. Eychmüller, *Angew. Chem., Int. Ed.* **2017**, *56*, 13200.
[5] L. Altenschmidt, S. Sánchez-Paradinas, F. Lübkemann, D. Zámbó, A. M. Abdelmonem, H. Bradtmüller, A. Masood, I. Morales, P. De La Presa, A. Knebel, M. A. G. García-Tuñón, B. Pelaz, K. D. J. Hindricks, P. Behrens, W. J. Parak, N. C. Bigall, *ACS Appl. Nano Mater.* **2021**, *4*, 6678.
[6] B. Cai, V. Sayevich, N. Gaponik, A. Eychmüller, *Adv. Mater.* **2018**, *30*, 1707518.
[7] A. Freytag, S. Sánchez-Paradinas, S. Naskar, N. Wendt, M. Colombo, G. Pugliese, J. Poppe, C. Demirci, I. Kretschmer, D. W. Bahnemann, P. Behrens, N. C. Bigall, *Angew. Chem., Int. Ed.* **2016**, *55*, 1200.
[8] A. Freytag, M. Colombo, N. C. Bigall, *Z. Phys. Chem.* **2017**, *231*, 63.
[9] D. Müller, L. F. Klepzig, A. Schlosser, D. Dorfs, N. C. Bigall, *Langmuir* **2021**, *37*, 5109.
[10] X. Ma, X. Sun, D. Hargrove, J. Chen, D. Song, Q. Dong, X. Lu, T.-H. Fan, Y. Fu, Y. Lei, *Sci. Rep.* **2016**, *6*, 19370.
[11] D. Govindarajan, N. Duraipandy, K. V. Srivatsan, R. Lakra, P. S. Korapatti, R. Jayavel, M. S. Kiran, *ACS Appl. Mater. Interfaces* **2017**, *9*, 16939.
[12] D. Wang, M. Wagner, H.-J. Butt, S. Wu, *Soft Matter* **2015**, *11*, 7656.
[13] N. Vadodariya, R. Meena, *ACS Sustainable Chem. Eng.* **2019**, *7*, 4814.
[14] I. Selmer, C. Kleemann, U. Kulozik, S. Heinrich, I. Smirnova, *J. Supercrit. Fluids* **2015**, *106*, 42.
[15] K. Ganesan, T. Budtova, L. Ratke, P. Gurikov, V. Baudron, I. Preibisch, P. Niemeyer, I. Smirnova, B. Milow, *Materials* **2018**, *11*, 2144.

[16] K. Ganesan, L. Ratke, *Soft Matter* **2014**, *10*, 3218.
[17] F. P. Soorbaghi, M. Isanejad, S. Salatin, M. Ghorbani, S. Jafari, H. Derakhshankhah, *Biomed. Pharmacother.* **2019**, *111*, 964.
[18] C. A. García-González, M. Alnaief, I. Smirnova, *Carbohydr. Polym.* **2011**, *86*, 1425.
[19] L. E. Nita, A. Ghilan, A. G. Rusu, I. Neamtu, A. P. Chiriac, *Pharmaceutics* **2020**, *12*, 449.
[20] S. Zhao, W. J. Malfait, N. Guerrero-Alburquerque, M. M. Koebel, G. Nyström, *Angew. Chem., Int. Ed.* **2018**, *57*, 7580.
[21] Y. Y. Shim, B. Gui, P. G. Arnison, Y. Wang, M. J. T. Reaney, *Trends Food Sci. Technol.* **2014**, *38*, 5.
[22] V. Perreault, L. Hénaux, L. Bazinet, A. Doyen, *Food Chem.* **2017**, *221*, 1805.
[23] M. H. H. Tehrani, R. Batal, M. Kamalinejad, A. Mahbubi, *J. Plant Sci.* **2014**, *2*, 70.
[24] B. Wang, L.-J. Wang, D. Li, B. Adhikari, J. Shi, *Carbohydr. Polym.* **2011**, *86*, 343.
[25] K. R. Kuhn, F. G. D. E. Silva, F. M. Netto, R. L. D. Cunha, *Food Res. Int.* **2014**, *58*, 89.
[26] B. Wang, D. Li, L.-J. Wang, B. Adhikari, J. Shi, *J. Food Eng.* **2010**, *100*, 417.
[27] M. Tirgar, P. Silcock, A. Carne, E. J. Birch, *Food Chem.* **2017**, *215*, 417.
[28] M. H. Alu'datt, T. Rababah, M. N. Alhamad, S. Gammoh, K. Ereifej, S. Kubow, I. Alli, *Food Hydrocolloids* **2016**, *61*, 119.
[29] A. Slavova-Kazakova, M. Karamać, V. Kancheva, R. Amarowicz, *Molecules* **2016**, *21*, 17.
[30] M. Loginov, N. Boussetta, N. Lebovka, E. Vorobiev, *J. Membr. Sci.* **2013**, *442*, 177.
[31] C. C. Udenigwe, A. P. Adebiyi, A. Doyen, H. Li, L. Bazinet, R. E. Aluko, *Food Chem.* **2012**, *132*, 468.
[32] C. C. Udenigwe, Y.-S. Lin, W.-C. Hou, R. E. Aluko, *J. Funct. Foods* **2009**, *1*, 199.
[33] H. K. Marambe, P. J. Shand, J. P. D. Wanasundara, *J. Agric. Food Chem.* **2011**, *59*, 9596.
[34] P. Kajla, A. Sharma, D. R. Sood, *J. Food Sci. Technol.* **2015**, *52*, 1857.
[35] R. Naran, G. Chen, N. C. Carpita, *Plant Physiol.* **2008**, *148*, 132.
[36] M. Feng, L. Pan, X. Yang, J. Sun, X. Xu, G. Zhou, *LWT–Food Sci. Technol.* **2018**, *87*, 361.
[37] H.-H. Chen, S.-Y. Xu, Z. Wang, *J. Food Eng.* **2006**, *77*, 295.
[38] E. Azarpazhooh, H. Rashidi, P. Sharayei, H. Behmadi, H. S. Ramaswamy, *Food Hydrocolloids Health* **2021**, *1*, 100017.
[39] Y. Liu, Z. Liu, X. Zhu, X. Hu, H. Zhang, Q. Guo, R. Y. Yada, S. W. Cui, *Compr. Rev. Food Sci. Food Saf.* **2021**, *20*, 2534.
[40] J. Liu, Y. Y. Shim, J. Shen, Y. Wang, M. J. T. Reaney, *Food Hydrocolloids* **2017**, *64*, 18.
[41] Y. Wang, D. Li, L.-J. Wang, B. Adhikari, *J. Food Eng.* **2011**, *104*, 56.
[42] S. Khalloufi, M. Corredig, H. D. Goff, M. Alexander, *Food Hydrocolloids* **2009**, *23*, 611.
[43] S. Nybroe, A. Astrup, C. R. Bjørnvad, *Int. J. Obes.* **2016**, *40*, 1884.
[44] M. Bustamante, B. D. Oomah, M. Rubilar, C. Shene, *Food Chem.* **2017**, *216*, 97.
[45] L. M. Comin, F. Temelli, M. D. A. Saldaña, *Innovative Food Sci. Emerging Technol.* **2015**, *28*, 40.
[46] E. C. Dreaden, A. M. Alkilany, X. Huang, C. J. Murphy, M. A. El-Sayed, *Chem. Soc. Rev.* **2012**, *41*, 2740.
[47] K. E. Fong, L.-Y. L. Yung, *Nanoscale* **2013**, *5*, 12043.
[48] J. Kobak, T. Smoleński, M. Goryca, M. Papaj, K. Gietka, A. Bogucki, M. Koperski, J.-G. Rousset, J. Suffczyński, E. Janik, M. Nawrocki, A. Golnik, P. Kossacki, W. Pacuski, *Nat. Commun.* **2014**, *5*, 3191.
[49] D. I. Son, B. W. Kwon, D. H. Park, W.-S. Seo, Y. Yi, B. Angadi, C.-L. Lee, W. K. Choi, *Nat. Nanotechnol.* **2012**, *7*, 465.
[50] W. M. O. S. De Santana, B. L. Caetano, S. R. De Annunzio, S. H. Pulcinelli, C. Ménager, C. R. Fontana, C. V. Santilli, *Colloids Surf., B* **2020**, *196*, 111297.
[51] D. H. Hanna, G. R. Saad, *RSC Adv.* **2020**, *10*, 20724.
[52] S. Jungblut, A. Eychmüller, in *Chemical Modelling*, Vol. 15 (Eds: M. Springborg, J.-O. Joswig), Royal Society of Chemistry, London, UK **2019**, pp. 1–27.
[53] K. Karrai, R. J. Warburton, C. Schulhauser, A. Högele, B. Urbaszek, E. J. Mcghee, A. O. Govorov, J. M. Garcia, B. D. Gerardot, P. M. Petroff, *Nature* **2004**, *427*, 135.
[54] L. Qu, X. Peng, *J. Am. Chem. Soc.* **2002**, *124*, 2049.
[55] S. Kumar, T. Nann, *Small* **2006**, *2*, 316.
[56] W. Chen, H. Yu, Q. Li, Y. Liu, J. Li, *Soft Matter* **2011**, *7*, 10360.
[57] Y. Chen, L. Zhou, L. Chen, G. Duan, C. Mei, C. Huang, J. Han, S. Jiang, *Cellulose* **2019**, *26*, 6653.
[58] Y. Chen, L. Zhang, Y. Yang, B. Pang, W. Xu, G. Duan, S. Jiang, K. Zhang, *Adv. Mater.* **2021**, *33*, 2005569.
[59] J. Šubrt, E. Pližingrová, M. Palkovská, J. Boháček, M. Klementová, J. Kupčík, P. Bezdička, H. Sovová, *Pure Appl. Chem.* **2017**, *89*, 501.
[60] W. Liao, H.-B. Zhao, Z. Liu, S. Xu, Y.-Z. Wang, *Composites, Part B* **2019**, *173*, 107036.
[61] D. Müller, A. Freytag, N. Bigall, *ECS Meet. Abstr.* **2018**, *MA2018-02*, 601.
[62] N. Buchtová, C. Pradille, J.-L. Bouvard, T. Budtova, *Soft Matter* **2019**, *15*, 7901.
[63] C. Rudaz, R. Courson, L. Bonnet, S. Calas-Etienne, H. Sallée, T. Budtova, *Biomacromolecules* **2014**, *15*, 2188.
[64] J. Liu, J. Shen, Y. Y. Shim, M. J. T. Reaney, *Int. J. Food Sci. Technol.* **2016**, *51*, 530.
[65] C. Burgos-Díaz, M. Rubilar, E. Morales, C. Medina, F. Acevedo, A. M. Marqués, C. Shene, *Eur. J. Lipid Sci. Technol.* **2016**, *118*, 165.
[66] N. S. Prado, I. S. V. D. Silva, T. A. L. Silva, W. J. D. Oliveira, L. A. D. C. Motta, D. Pasquini, H. Otaguro, *Mater. Res.* **2018**, *21*.
[67] R. Devi, M. Bhatia, *Int. J. Biol. Macromol.* **2019**, *126*, 101.
[68] E. Lopez-Gonzalez, C. Saiz-Arroyo, M. A. Rodriguez-Perez, *Int. J. Environ. Sci. Technol.* **2020**, *17*, 1663.
[69] C. R. R., S. P. Sundaran, A. J., S. Athiyanathil, *RSC Adv.* **2017**, *7*, 2092.
[70] T. Zhang, Z. Li, Y. Lü, Y. Liu, D. Yang, Q. Li, F. Qiu, *Chin. J. Chem. Eng.* **2019**, *27*, 1282.
[71] Z. Li, L. Shao, W. Hu, T. Zheng, L. Lu, Y. Cao, Y. Chen, *Carbohydr. Polym.* **2018**, *191*, 183.
[72] L. Sun, Z. Jiang, B. Yuan, S. Zhi, Y. Zhang, J. Li, A. Wu, *Chem. Eng. Res. Des.* **2021**, *174*, 71.
[73] B. He, Y. Zhang, B. Li, Y. Chen, L. Zhu, *J. Environ. Chem. Eng.* **2021**, *9*, 106333.
[74] Z. Yin, X. Sun, M. Bao, Y. Li, *Int. J. Biol. Macromol.* **2020**, *165*, 1869.
[75] L. Yi, Y. Xia, Z. Tan, X. Fang, L. Zhao, H. Wu, S. Guo, *J. Cleaner Prod.* **2020**, *264*, 121558.
[76] Y. Lu, Y. Wang, L. Liu, W. Yuan, *Carbohydr. Polym.* **2017**, *173*, 422.
[77] J. Wang, Y. Zheng, A. Wang, *Chem. Eng. J.* **2012**, *213*, 1.
[78] P. K. Renjith, C. Sarathchandran, V. Sivanandan Achary, N. Chandramohanakumar, V. Sekkar, *J. Hazard. Mater.* **2021**, *415*, 125548.
[79] G. Shi, Y. Qian, F. Tan, W. Cai, Y. Li, Y. Cao, *R. Soc. Open Sci.* **2019**, *6*, 181823.
[80] L. Liu, G. Kong, Y. Zhu, C. Che, *Colloid Interface Sci. Commun.* **2021**, *45*, 100518.
[81] A. A. Pawar, A. Kim, H. Kim, *Environ. Pollut.* **2021**, *288*, 117717.
[82] Q. B. Thai, D. K. Le, N. H. N. Do, P. K. Le, N. Phan-Thien, C. Y. Wee, H. M. Duong, *J. Environ. Chem. Eng.* **2020**, *8*, 104016.
[83] X. Shi, Y. Lan, S. Peng, Y. Wang, J. Ma, *ACS Omega* **2020**, *5*, 14232.
[84] H. Bidgoli, Y. Mortazavi, A. A. Khodadadi, *J. Hazard. Mater.* **2019**, *366*, 229.
[85] Z.-L. Ma, X.-L. Wang, H.-M. Wei, H.-Z. Song, *J. Appl. Polym. Sci.* **2015**, *132*, 41244.
[86] H. Cheng, B. Gu, M. P. Pennefather, T. X. Nguyen, N. Phan-Thien, H. M. Duong, *Mater. Des.* **2017**, *130*, 452.
[87] L. Manzocco, K. S. Mikkonen, C. A. García-González, *Food Struct.* **2021**, *28*, 100188.

[88] A. Li, R. Lin, C. Lin, B. He, T. Zheng, L. Lu, Y. Cao, *Carbohydr. Polym.* **2016**, *148*, 272.
[89] C. Jin, S. Han, J. Li, Q. Sun, *Carbohydr. Polym.* **2015**, *123*, 150.
[90] J. Yue, G. Wen, G. Ren, S. Tang, B. Ge, L. Zhao, X. Shao, *Langmuir* **2021**, *37*, 406.
[91] J. Wei, S.-H. Gui, J.-H. Wu, D.-D. Xu, Y. Sun, X.-Y. Dong, Y.-Y. Dai, Y.-F. Li, *Appl. Environ. Biotechnol.* **2019**, *4*, 11.
[92] C. Cao, J. Ren, Y.-K. Lv, R.-P. Ren, *Green Mater.* **2021**, *9*, 21.
[93] X. Wang, S. Nie, P. Zhang, L. Song, Y. Hu, *J. Mater. Res. Technol.* **2020**, *9*, 667.
[94] J.-H. Woo, Y.-H. Kim, Y.-J. Choi, D.-G. Kim, K.-S. Lee, J. H. Bae, D. S. Min, J.-S. Chang, Y.-J. Jeong, Y. H. Lee, J.-W. Park, T. K. Kwon, *Carcinogenesis* **2003**, *24*, 1199.
[95] S. Singh, R. Arya, R. R. Bargaje, M. K. Das, S. Akram, H. M. Faruquee, R. K. Behera, R. K. Nanda, A. Agrawal, *bioRxiv 721100* **2020**.
[96] M. Chen, Z.-Y. Du, X. Zheng, D.-L. Li, R.-P. Zhou, K. Zhang, *Neural Regener. Res.* **2018**, *13*, 742.
[97] V. S. Patil, A. M. Gutierrez, M. Sunkara, A. J. Morris, J. Z. Hilt, D. S. Kalika, T. D. Dziubla, *J. Nat. Prod.* **2017**, *80*, 1964.
[98] D. Sinha, D. De, A. Ayaz, *Spectrochim. Acta, Part A* **2018**, *193*, 467.
[99] S. Ilic, V. Paunovic, *Facta Univ., Ser.: Electron. Energ.* **2019**, *32*, 91.
[100] S. J. Yoon, I. Lim, J. H. Kim, S. Adhikari, W. Y. Lee, J. K. Lee, N. K. Shrestha, H. Ahn, J. W. Han, S.-H. Han, *Energy Sources, Part A* **2016**, *38*, 183.
[101] K. T. Kazantzis, K. Koutsonikoli, B. Mavroidi, M. Zachariadis, P. Alexiou, M. Pelecanou, K. Politopoulos, E. Alexandratou, M. Sagnou, *Photochem. Photobiol. Sci.* **2020**, *19*, 193.
[102] L. Zhang, P. Wang, Z. Yang, F. Du, Z. Li, C. Wu, A. Fang, X. Xu, G. Zhou, *Food Hydrocolloids* **2020**, *101*, 105455.
[103] M. Zhou, T. Wang, Q. Hu, Y. Luo, *Food Hydrocolloids* **2016**, *57*, 20.
[104] P. P. Nerkar, S. Gattani, *Drug Delivery* **2011**, *18*, 111.
[105] H. Wang, Z. Shao, M. Bacher, F. Liebner, T. Rosenau, *Cellulose* **2013**, *20*, 3007.
[106] V. R. Marinov, I. T. Lima Jr., R. Miller, in *Three-Dimensional Imaging, Visualization, and Display 2010 and Display Technologies and Applications for Defense, Security, and Avionics IV* (Eds: B. Javidi, J.-Y. Son, J. T. Thomas, D. D. Desjardins), SPIE, Bellingham, WA **2010**, p. 76900X.
[107] D. Zámbó, A. Schlosser, P. Rusch, F. Lübkemann, J. Koch, H. Pfnür, N. C. Bigall, *Small* **2020**, *16*, 1906934.
[108] S. Sánchez-Paradinas, D. Dorfs, S. Friebe, A. Freytag, A. Wolf, N. C. Bigall, *Adv. Mater.* **2015**, *27*, 6152.
[109] M. Li, Y. Wang, A. Chen, A. Naidu, B. S. Napier, W. Li, C. L. Rodriguez, S. A. Crooker, F. G. Omenetto, *Proc. Natl. Acad. Sci. U. S. A.* **2018**, *115*, 8119.
[110] Y. Li, Q. Liu, A. J. Hess, S. Mi, X. Liu, Z. Chen, Y. Xie, I. I. Smalyukh, *ACS Nano* **2019**, *13*, 13875.
[111] Y. Li, X. Liu, X. Nie, W. Yang, Y. Wang, R. Yu, J. Shui, *Adv. Funct. Mater.* **2019**, *29*, 1807624.
[112] H. Gu, X. Zhou, S. Lyu, D. Pan, M. Dong, S. Wu, T. Ding, X. Wei, I. Seok, S. Wei, Z. Guo, *J. Colloid Interface Sci.* **2020**, *560*, 849.
[113] S. Kolev, T. Koutzarova, in *Nanoscience and Nanotechnology in Security and Protection against CBRN Threats* (Eds.: P. Petkov, M. E. Achour, C. Popov), Springer, Dordrecht **2020**, pp. 251–257.
[114] Z. Wu, K. Pei, L. Xing, X. Yu, W. You, R. Che, *Adv. Funct. Mater.* **2019**, *29*, 1901448.
[115] M. M. Abdellatif, S. M. A. Soliman, N. H. El-Sayed, F. H. H. Abdellatif, *J. Porous Mater.* **2020**, *27*, 277.
[116] Y. Guan, J. Rao, Y. Wu, H. Gao, S. Liu, G. Chen, F. Peng, *Int. J. Biol. Macromol.* **2020**, *155*, 369.
[117] J. Cai, Y. Q. Miao, B. Z. Yu, P. Ma, L. Li, H. M. Fan, *Langmuir* **2017**, *33*, 1662.
[118] K. Davis, B. Cole, M. Ghelardini, B. A. Powell, O. T. Mefford, *Langmuir* **2016**, *32*, 13716.
[119] L. Carbone, C. Nobile, M. De Giorgi, F. D. Sala, G. Morello, P. Pompa, M. Hytch, E. Snoeck, A. Fiore, I. R. Franchini, M. Nadasan, A. F. Silvestre, L. Chiodo, S. Kudera, R. Cingolani, R. Krahne, L. Manna, *Nano Lett.* **2007**, *7*, 2942.
[120] T. Kodanek, H. M. Banbela, S. Naskar, P. Adel, N. C. Bigall, D. Dorfs, *Nanoscale* **2015**, *7*, 19300.
[121] L. Zhongfa, M. Chiu, J. Wang, W. Chen, W. Yen, P. Fan-Havard, L. D. Yee, K. K. Chan, *Cancer Chemother. Pharmacol.* **2012**, *69*, 679.
[122] N. G. Kotla, O. Burke, A. Pandit, Y. Rochev, *Nanomaterials* **2019**, *9*, 1246.

